ORIGINAL RESEARCH

Exosome-Delivered circFOXP1 Upregulates Autophagy and Promotes Hepatocellular Carcinoma Progression Through Its Encoded p196 Protein Targeting the KHDRBS3/ULK1 Axis

Peng Zhao*, Chuanzheng Yin*, Ran Liu*, Shuyu Shao, Wenbo Ke, Zifang Song

Department of Hepatobiliary Surgery, Union Hospital, Tongji Medical College, Huazhong University of Science and Technology, Wuhan, Hubei, 430022, People's Republic of China

*These authors contributed equally to this work

Correspondence: Zifang Song, Email zsong@hust.edu.cn

Introduction: Circular RNAs (circRNAs) are pivotal regulators in cancer, and circFOXP1 has been implicated in tumorigenesis. This study explores the exosome-mediated transfer of circFOXP1 and its functional protein product, p196, in hepatocellular carcinoma (HCC) progression.

Methods: HCC circRNA datasets were obtained from the Gene Expression Omnibus (GEO) databases, and circRNAs were validated via qRT-PCR and Sanger sequencing. Exosomes were isolated via ultracentrifugation and characterized by TEM/NTA. RIP, Co-IP, RNA pull-down and in vitro binding assays were employed to determine molecular interactions. Loss- and gain-of-function assays were employed to evaluate the effects of circFOXP1, KHDRBS3 and ULK1 on the proliferation, and invasion abilities of HCC cells both in vitro and in vivo.

Results: CircFOXP1, which encoded a 196-amino acid protein, p196, was highly expressed in HCC tissues and cells and secreted via exosomes. Overexpression of p196 enhanced HCC cell proliferation, invasion, and autophagy flux in vitro, while knockdown produced opposite effects. Mechanistically, p196 directly bound KHDRBS3 through its D2 domain, forming a complex that stabilized ULK1 mRNA, thereby increasing ULK1 protein levels, activating autophagy and accelerating tumor progression.

Conclusion: Our findings indicated that circFOXP1-encoded p196 plays a role as a tumor promoter, contributing to the malignant progression of HCC. Targeting the circFOXP1/p196-KHDRBS3-ULK1 axis presents a promising therapeutic strategy for HCC, with potential applications in biomarker development and combination therapies.

Keywords: hepatocellular carcinoma, exosomes, circular RNAs, KHDRBS3, ULK1, autophagy

Introduction

Liver cancer represents a substantial global health challenge, accounting for alarmingly high morbidity and mortality rates worldwide. It stands as the third most common cause of cancer-related deaths, with an annual incidence of over 900,000 new cases and leading to more than 800,000 fatalities.[1,2] Hepatocellular carcinoma (HCC) accounts for approximately 90% of all liver cancer cases, with intrahepatic cholangiocarcinoma (ICC) and combined hepatocellular-cholangiocarcinoma (CHC) following in incidence.[3] A significant proportion of liver cancer patients are diagnosed at advanced stages, underscoring the pressing requirement for efficacious anticancer therapies. However, owing to the marked heterogeneity and complexity inherent to liver cancer, the majority of drugs targeted at this malignancy have failed to demonstrate efficacy in clinical trials.[2] Current therapeutic modalities for liver cancer encompass transarterial chemoembolization (TACE) and multi-target kinase inhibitors, yet the survival advantages conferred by these treatments remain limited.[4] Recent clinical trials have reported initial favorable responses in a minor segment of HCC patients who

received combined anti-angiogenic and immune checkpoint inhibitor therapies. Nonetheless, these patients ultimately exhibit drug resistance,[4] emphasizing the critical necessity to elucidate the underlying molecular mechanisms propelling liver cancer progression and to devise innovative therapeutic approaches.

Circular RNAs (circRNAs) constitute a distinct class of non-coding RNAs, distinguished by their absence of 5′ end caps and 3′ poly(A) tails, which enables them to form covalently closed circular configurations.[5] A growing body of evidence indicates that the aberrant expression of circRNAs is widespread across nearly all cancer types, where they exert regulatory functions over multiple facets of tumor biology, encompassing the immune microenvironment, metabolic reprogramming, proliferation, invasion, migration, apoptosis, and drug resistance.[6,7] In the specific context of liver cancer, circRNAs have been implicated as playing crucial roles. For instance, exosome-derived circCCAR1 has been demonstrated to induce CD8+ T cell dysfunction and anti-PD1 resistance in HCC.[8] Conversely, circular RNA-YBX1 has been shown to inhibit liver cancer metastasis through a mechanism involving phase separation-mediated cytoskeletal remodeling.[9] Furthermore, circPSD3 acts as an inhibitor of the urokinase-type plasminogen activator (uPA) system, thereby suppressing vascular invasion and metastasis in HCC.[10]

Exosomes are small single-membrane secretory organelles with a diameter ranging from approximately 30 to 200 nanometers,[11] functioning as natural nanovesicles that mediate intercellular communication.[12,13] Through exosomes, donor cells can transfer exogenous materials such as proteins, messenger RNAs (mRNAs), microRNAs (miRNAs), and lipids to recipient cells, playing roles in various biological and pathological processes.[12–14] Moreover, numerous studies have shown that circular RNAs (circRNAs) are enriched in exosomes and regulate tumor progression through inter-cellular transmission via exosomes.[15–17] However, how exosome-delivered circRNAs participate in the regulation of HCC progression remains unknown.

Recent pioneering research has provided further insights into the coding potential of certain circRNAs, revealing their capacity to encode functional peptides or proteins. Specifically, circDIDO1 has been found to hinder gastric cancer progression by encoding a novel protein, DIDO1-529aa.[18] Similarly, circMTHFD2L exerts an inhibitory effect on GC progression through the encoding of CM-248aa.[19] In parallel, a polypeptide encoded by circular RNA ZKSCAN1 has been demonstrated to suppress HCC by facilitating the degradation of mTOR.[20] Despite these advancements, the roles and underlying mechanisms of circRNA-encoded proteins in HCC remain largely uncharted territories.

Autophagy represents an evolutionarily conserved intracellular catabolic process that entails the delivery of cyto-plasmic macromolecules, aggregated proteins, damaged organelles, and pathogens to lysosomes for enzymatic digestion by lysosomal hydrolases. This process results in the generation of nucleotides, amino acids, fatty acids, sugars, and adenosine triphosphate (ATP), which are subsequently recycled into the cytoplasm. This mechanism facilitates the recycling and renewal of organelles, thereby maintaining cellular homeostasis.[21,22] Autophagy exerts multifaceted effects on the initiation and progression of HCC. For example, elevated levels of p62 activate Nrf2, thereby protecting HCC-initiating cells from cell death induced by oxidative stress.[23] Additionally, the induction of autophagy in HCC promotes cancer growth through the activation of the JNK/Bcl2[24] and Wnt signaling pathways.[25] Moreover, the inhibition of autophagy enhances the sensitivity of HCC cells to sorafenib treatment.[26,27] It is noteworthy that the expression of autophagy-related markers, such as LC3 and ULK1, has been linked to poor prognosis in HCC patients following surgical resection.[28–30] Among the Atg genes that encode ATG proteins involved in coordinating autophagy-related processes, ULK1, a proximal gene responsible for initiating autophagy, has attracted significant attention owing to its druggability and its non-canonical, non-autophagy-dependent roles.[31,32]

In this study, we found that circFOXP1 can be packaged and transmitted by exosomes, and we identified a novel 196 amino acid protein named p196, which is encoded by circFOXP1 and functions as a newly discovered tumor promoter in HCC. Functionally, p196 exerts a promotive effect on the growth and metastasis of HCC cells, as well as on autophagy, both in vitro and in vivo. Mechanistically, p196 interacts with KHDRBS3 by binding to its D2 domain. This interaction subsequently facilitates the binding of the complex to ULK1 mRNA, thereby enhancing its stability and upregulating autophagy levels. These findings indicate that p196 plays a role as a tumor promoter, contributing to the malignant progression of HCC. Consequently, p196 may represent a potential therapeutic target for the treatment of HCC.

Materials and Methods

Clinical Specimens

From May 2019 to December 2023, HCC tumor tissues and adjacent non-tumor tissues were obtained from Union Hospital, affiliated with Tongji Medical College of Huazhong University of Science and Technology. The samples were collected from 70 males and 15 females, aged between 23 and 84 years (mean age: 59.1 years), who had not received any anticancer treatment prior to surgery. This study was approved by the Ethics Committee of Union Hospital in accordance with the Declaration of Helsinki. All tissue donors provided written informed consent.

Cell Lines

The human normal liver cell line (MIHA) and HCC cell lines (SNU449, Hep3B, Huh7, MHCC97-H) were purchased from the American Type Culture Collection (ATCC, Manassas, VA, USA). All cell lines were cultured in Dulbecco's Modified Eagle Medium (DMEM; Gibco, Carlsbad, CA, USA) containing 10% fetal bovine serum (FBS; Sigma-Aldrich, St. Louis, MO, USA) and 100 U/mL penicillin at 37°C in a humidified atmosphere with 5% CO2. All cell lines were tested for Mycoplasma contamination every 6 months using EZ-PCR mycoplasma test kit (Biological industries).

Cell Transfection

The circFOXP1 overexpression vector was constructed by GenePharma (Shanghai, China), utilizing the pLC5-ciR vector as a negative control. For the knockdown of circFOXP1 or ULK1, specific short hairpin RNAs (shRNAs) were designed to target the splicing sites of circFOXP1 (sh-circFOXP1#1 and sh-circFOXP1#2), ULK1 (sh-ULK1-1 and sh-ULK1-2), and KHDRBS3 (sh-KHDRBS3). These shRNAs were subsequently cloned into the pLKO.1 plasmid. HCC cells were plated in six-well plates at a density of 3×10^4 cells per well. Plasmid transfection was executed using Lipofectamine 3000 (Invitrogen, Carlsbad, CA, USA) in accordance with the manufacturer's protocol. Briefly, the plasmid was initially mixed with Opti-MEM (Invitrogen) and incubated for 5 minutes, followed by co-incubation with Lipofectamine 3000 for 20 minutes prior to transfection into the cells. After 72 hours, the cells were harvested for subsequent analysis.

Tumor Xenograft Assay

The animal experimentation protocol was approved by the Animal Care and Use Committee of Tongji Medical College, Huazhong University of Science and Technology. Male BALB/c nude mice, aged 6 weeks, were obtained from Hubei Biotech Co., Ltd. (Wuhan, China) and maintained under specific pathogen-free (SPF) conditions. The mice were randomly assigned to two groups, namely Vector and circFOXP1. Subsequently, 5×10^6 HCC cells were subcutaneously injected into the flank of nude mice (5 mice in each group). Tumor volume measurements were recorded at 7-day intervals. Following a 28-day period, the mice were euthanized, and the tumors were weighed and photographed for further analysis.

Bioinformatic Analysis

To identify the target circRNA, a comprehensive search was conducted within the Gene Expression Omnibus (GEO) database using the search terms "(circRNA* OR circular) AND (liver cancer OR hepatic carcinoma OR hepatocarcinoma)" up to April 2023. This search resulted in the inclusion of seven datasets (accession numbers: GSE242797, GSE166678, GSE121714, GSE155949, GSE94508, GSE97332, and GSE174179) in our study. After removing duplicate records, a combined dataset comprising 92 hCC samples and 82 adjacent normal tissue samples was compiled. Preprocessing of the raw datasets was performed using the "limma" R package, and all circRNA names were standardized according to circBase. In cases where duplicate genes were present, their expression values were averaged. To identify differentially expressed circular RNAs (DECs) between liver cancer and adjacent normal tissues, the MetaDE package was employed. For the integrated analysis, filtering thresholds for the mean and standard deviation (SD) were set at 10%. To address the varying levels of stringency in the methodologies, Fisher's test was utilized. Additionally, modified t-tests and permutation methods were applied to derive P-values, ensuring the rigor and accuracy of our analysis.

Real-Time Quantitative PCR

Total RNA and genomic DNA (gDNA) were extracted from cells or tissues utilizing the RNeasy Mini Kit and DNA Mini Kit (QIAGEN, Hilden, Germany), respectively, in accordance with the manufacturer's protocols. The extracted RNA was then reverse-transcribed into cDNA using the PrimeScript RT enzyme Mix (TaKaRa, Kusatsu, Japan). The primers employed for the quantification of mRNA, circular RNA (circRNA), and gDNA are detailed in Table S1. The expression levels of circRNAs and mRNA were normalized to GAPDH, and quantification was performed using the $2^{-\Delta\Delta Ct}$ method. Each experiment was conducted in triplicate to ensure reproducibility.

Fluorescence in situ Hybridization (FISH)

A biotin-labeled probe, specific for circFOXP1, was synthesized by RiboBio Technology Co. (located in Guangzhou, China). RNA FISH assays were carried out using the Fluorescence In Situ Hybridization Kit (product code C10910, RiboBio), strictly adhering to the manufacturer's instructions. Observations and image capture were executed using a confocal laser scanning microscope (model LSM 780 with Airyscan, manufactured by Carl Zeiss in Oberkochen, Germany).

Western Blot Analysis

Total protein extraction from cells was achieved using RIPA lysis buffer (P0013B, Beyotime, Shanghai, China). The proteins were subsequently separated by electrophoresis on 10% tri-glycine gels and transferred onto polyvinylidene fluoride (PVDF) membranes (MilliporeSigma, Burlington, MA, USA). The membranes were then blocked with 5% skim milk at room temperature for 1 hour, followed by overnight incubation with the specified primary antibodies: anti-FOXP1 (NBP1-89410, Novus Biologicals, Littleton, CO, USA), anti-Cyclin D1 (26,939-1-AP, Proteintech, Rosemont, IL, USA), anti-CDK4 (11,026-1-AP, Proteintech), anti-MMP9 (27,306-1-AP, Proteintech), anti-Vimentin (10366-1-AP, Proteintech), anti-N-cadherin (22018-1-AP, Proteintech), anti-E-cadherin (20874-1-AP, Proteintech), anti-ULK1 (20,986-1-AP, Proteintech), anti-KHDRBS3 (13,563-1-AP, Proteintech), anti-GAPDH (60004-1-Ig, Proteintech), anti-myc tag (16286-1-AP, Proteintech), anti-Flag tag (20543-1-AP, Proteintech), and anti-LC3B (ab192890, Abcam, Cambridge, UK), anti-HSP70 (10,995-1-AP, Proteintech), anti-TSG101 (28,283-1-AP, Proteintech), anti-CD63 (25,682-1-AP, Proteintech), anti-CD9 (20,597-1-AP, Proteintech). After three washes with TBST, goat anti-rabbit IgG-HRP antibody (ab6721, Abcam) was applied as the secondary antibody. The membranes were subsequently washed twice with PBST and once with PBS, each wash lasting 10 minutes, and finally visualized using an enhanced chemiluminescence system (Millipore).

Proteomics Analysis

For each sample, an aliquot of 5 micrograms of protein was taken, and a single sample was used for the preparation of the peptide library. The spectral library was generated using liquid chromatography-mass spectrometry (LC-MS) technology. Quantitative analysis of the samples was performed by sequential window acquisition of all theoretical fragment ion spectra (SWATH-MS). The SWATH quantitative data then underwent median normalization followed by Log2 transformation. Proteins were considered differentially expressed if they had a p-value < 0.01, as determined by the Student's *t*-test.

Co-Immunoprecipitation Assay

The cell lysate was prepared using cytolysis buffer designed for immunoprecipitation (IP) (Beyotime) and adjusted to achieve a final concentration of 1 μg/μL. A portion of approximately 10% of the cell lysate served as the input group. For the co-immunoprecipitation (Co-IP) group, Protein A agarose beads were introduced into the diluted cell supernatant and incubated at 4°C for 1 hour with constant stirring to minimize nonspecific background interference. Subsequently, the cell extracts were combined with either control IgG (Cell Signaling Technology, Danvers, MA, USA) or the specific antibody at a concentration of 4 μg/mL and incubated on a rotating platform at 4°C overnight. Following this, Protein A/G plus-agarose (Santa Cruz Biotechnology, Dallas, TX, USA) was added, and the mixture was further incubated for an

additional 2 hours at 4°C with stirring. Afterward, the agarose beads were isolated, washed with lysis buffer, and an equivalent volume of each sample was analyzed by Western blotting.

RNA Immunoprecipitation (RIP) Assay

The RIP (RNA Immunoprecipitation) experiment was executed utilizing the Magna RIP RNA-Binding Protein Immunoprecipitation Kit (Millipore, Billerica, MA, USA), strictly adhering to the manufacturer's instructions. Cell lysate was prepared using a cell lysis buffer that incorporated RNase inhibitors and protease inhibitors to ensure RNA integrity. Prior to immunoprecipitation, the magnetic beads were pre-incubated with the designated antibody or IgG at room temperature for a duration of 40 minutes, subsequently washed with RIP wash buffer to remove unbound components. The immunoprecipitation procedure was carried out overnight at 4°C, employing bead-bound antibodies suspended in RIP immunoprecipitation buffer containing 0.5M EDTA and 5 μL of RNase inhibitor to prevent RNA degradation. Following the immunoprecipitation step, the magnetic beads were retained and subjected to repeated washing to eliminate nonspecific binding. The immunoprecipitate was then mixed with Salt Solution I, Salt Solution II, Precipitation Enhancer, and absolute ethanol, and incubated at −80°C overnight to facilitate RNA precipitation. Lastly, the samples were centrifuged at 14,000 rpm for 15 minutes at 4°C, washed with 80% ethanol to remove residual salts, resuspended in 10 to 20 μL of RNase-free water, and subsequently analyzed by qRT-PCR (quantitative reverse transcription polymerase chain reaction).

RNA Pull-Down Assay

The RNA pull-down assays were conducted using the Pierce™ RNA 3′ End Desthiobiotinylation Kit and the Pierce™ Magnetic RNA-Protein Pull-Down Kit, both of which were obtained from Thermo Scientific (USA). These assays were performed in strict adherence to the manufacturer's instructions. Subsequently, the protein complexes that were bound to the RNA were subjected to analysis via Western blotting. To conclude the experimental protocol, mass spectrometry (MS) analysis was expertly executed by SpecAlly Life Technology Co., Ltd., located in Wuhan, China.

Colony Formation Assays

HCC cells in the logarithmic growth phase were harvested from monolayer cultures and subsequently digested with 0.25% trypsin. The cells were then dispersed into individual units and suspended in DMEM medium supplemented with 10% fetal bovine serum. A suspension of these digested HCC cells, containing 2000 cells per well, was seeded into a 6-well plate with 2 mL of medium and incubated at 37°C under conditions of 5% CO2 and saturated humidity for a duration of 2–3 weeks. Following this incubation period, the cells were fixed with 5 mL of methanol for 15 minutes. The culture was terminated upon the appearance of visible clones in the dish. An appropriate volume of 0.1% crystal violet was added and allowed to stand for 10–30 minutes. Subsequently, clones were counted either directly with the naked eye or under a microscope at low magnification, specifically noting clusters consisting of 50 or more cells.

Transwell Assay

HCC cells in the logarithmic growth phase were harvested from monolayer cultures and subjected to digestion with 0.25% trypsin, resulting in their dispersion into individual cells. Following this, the cells were suspended in DMEM medium supplemented with 10% fetal bovine serum. Subsequently, the cells were resuspended in serum-free medium, enumerated, and adjusted to achieve a cell density of 2.5×10^5 cells/mL. A volume of 700 microliters of conditioned medium, containing 30% FBS, was then added to the lower chamber. The Transwell chamber (Corning Life Sciences, Corning, NY, USA) was subsequently positioned within a 24-well plate. Each well of the upper chamber received 200 microliters of the cell suspension. After an incubation period of 20–24 hours at 37°C, the Transwell chamber was carefully removed and washed twice with PBS. Fixation was achieved using 4% paraformaldehyde at 4°C. The cells were then stained with 0.1% crystal violet. Observation of the cells was carried out under a microscope, and images were captured using ImageJ software (National Institutes of Health, Bethesda, MD, USA) for subsequent analysis.

Cell Cycle Assay

The distribution of the cell cycle was assessed utilizing flow cytometry. HCC cells in the growth phase were harvested, and 500μL of PBS was added to gently disperse any cell clumps into a suspension. While vortexing, 2 mL of cold 95% ethanol was gradually introduced at 20°C, and the cells were mixed and fixed for a duration of 30 minutes. Following this, 5 mL of PBS was added, and the cells were centrifuged at 1500 rpm for 5 minutes to remove the supernatant. This washing step was repeated once more with an additional 5 mL of PBS. Subsequently, 800 μL of propidium iodide staining solution was added, and the cell suspension was gently mixed using a pipette. The cells were then stained in the dark at room temperature for 30 minutes. Red fluorescence was detected using a flow cytometer (BD Biosciences, Franklin Lakes, NJ, USA) with an excitation wavelength set at 488 nm (PE channel).

Isolation and Characterization of Exosomes

Cells were cultured in exosome-depleted serum (Vivacell, Shanghai, China) to eliminate the interference of serum-derived exosomes. After 72 hours of culture, the medium was collected to extract exosomes. The supernatant was subjected to differential centrifugation at $500 \times g$ and $3000 \times g$ for 10 minutes, followed by pre-clarification using a 0.2 μm filter (MilliporeSigma). Exosomes were then pelleted by centrifugation at $120,000 \times g$ for 2 hours at 4°C, and resuspended in PBS for collection. Exosomes were imaged using an electron microscope (Thermo, Waltham, MA, USA). The size and quantity of exosomes were tracked and recorded using the NanoSight NS300 system (NanoSight Technology, Malvern, UK). GW4869, purchased from MedChemExpress (Catalog No: HY-19363), was incubated with cells at a concentration of 20 μM at 37°C for 30 minutes to inhibit exosome release.

Statistical Analysis

All in vitro experiments were conducted in triplicate to ensure reproducibility. Statistical analyses were carried out using GraphPad Prism 8, SPSS 23.0, and R 4.2.0 software. Unless otherwise stated, all variables are presented as the mean ± standard deviation. For comparisons between groups, Student's *t*-test was employed. All statistical tests were two-sided, with a significance level set at 0.05. Differences in statistical significance are denoted as follows: *$p < 0.05$, **$p < 0.01$, ***$p < 0.001$; Ns: not significant.

Results

CircFOXP1 is Upregulated in HCC Cells and Tissues, Exerting Tumorigenic Effects in HCC Cell Lines

The screening procedure for Differentially Expressed Circular RNAs (DECs) between HCC and adjacent normal tissues is depicted in Figure 1A. Figure 1B presents the number and combination of DECs, along with their corresponding p-values for each dataset. By integrating expression data from seven datasets, a total of 283 DECs were identified, from which the top 20 candidates, including hsa_circ_0004368 and hsa_circ_0000075, were selected for validation (Figure 1C). PCR amplification using distinct primers validated six circRNAs in HCC cell lines (Figure S1A). Sanger sequencing verified the circular structures of hsa_circ_0008234 (circFOXP1), hsa_circ_0003655 (circSND1), and hsa_circ_0005982 (circPTK2), which were in agreement with sequences in the circBase database (Figure 1D and E; Figure S1B–E). Further analysis revealed a significant upregulation of circFOXP1 in HCC tissues and cell lines, warranting further investigation into its functional role (Figure 1F and G; Figure S1F–I). The association of circFOXP1 expression with clinicopathological characteristics of HCC was presented in Table S2. Based on the high expression of circFOXP1 in MHCC97-H cells and the relatively low expression in Huh7 cells, these two cell lines were chosen for subsequent experimentation. Resistance to RNase R exonuclease digestion confirmed the circular nature of circFOXP1 (Figure 1H and I; Figure S1J and K), and FISH assays demonstrated its cytoplasmic enrichment in HCC cells (Figure 1I; Figure S1K). Functional gain-and-loss studies in Huh7 and MHCC97-H cells demonstrated satisfactory expression efficiency of circFOXP1 (Figure 1J). In vivo experiments revealed that circFOXP1 promoted tumor growth and weight in nude mice injected with Huh7 cells, with Ki-67 expression being upregulated upon circFOXP1
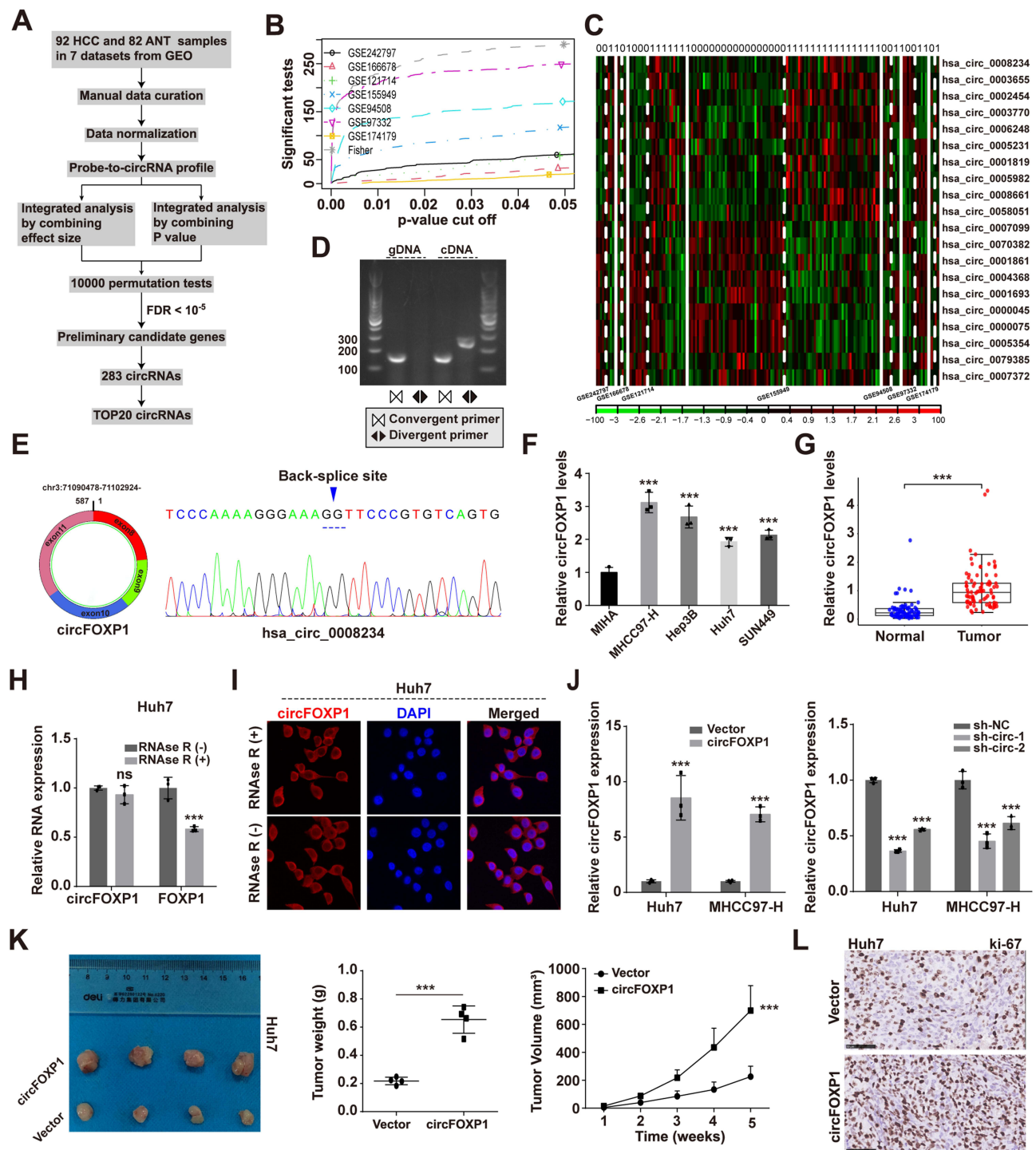
Figure 1 Characteristics of circFOXP1 in HCC. (**A**) Flowchart for screening differentially expressed circular RNAs (DECs) between HCC and adjacent normal tissues. (**B**) Ratio of DECs to p-values in the assessment of seven GEO datasets. (**C**) Heatmap identifying top 20 common DECs between HCC and adjacent samples across seven datasets. (**D**) hsa_circ_0008234 can be amplified by different cDNA primers but not from genomic DNA of Huh7 cells. (**E**) hsa_circ_0008234 is derived from the host gene FOXP1 and verified by Sanger sequencing. (**F** and **G**) RT-qPCR analysis of hsa_circ_0008234 expression levels in HCC cell lines (**F**) and tissues (**G**). **H**) RT-qPCR analysis of RNA levels of circFOXP1 and FOXP1 in Huh7 cells after RNase R treatment. (**I**) FISH assay showing cytoplasmic localization of circFOXP1 in Huh7 cells (green). Scale bar: 10 μm. (**J**) RT-qPCR analysis of circFOXP1 expression in Huh7 and MHCC97-H cells transfected with circFOXP1 expression vector, Vector control, sh-circFOXP1, or sh-NC. (**K**) Representative images, growth curves, and final weights of xenografts formed by subcutaneous transplantation of Huh7 cells stably transfected with Vector or circFOXP1 into the dorsal side of nude mice (n = 4 per group). (**L**) Representative images and quantitation of immunohistochemical staining for Ki-67 expression in xenografts formed by subcutaneous injection of Huh7 cells stably transfected with Vector or circFOXP1. Scale bars represent 50 μm. ***P<0.001, ns, not significant.

overexpression (Figure 1K and L). These findings suggest that circFOXP1 is upregulated in HCC cells and tissues, contributing to the proliferation of HCC cells.

CircFOXP1 Encodes a Novel Protein, the p196 Isoform, Comprising 196 Amino Acids

By utilizing the TransCirc database (accessible at https://www.biosino.org/transcirc/), we identified an internal ribosome entry site (IRES) and predicted an open reading frame (ORF) within circFOXP1, which potentially encodes a 196-amino acid polypeptide termed p196 (Figure 2A). The activity of the wild-type IRES was confirmed through a dual luciferase assay, which demonstrated higher Luc/Rluc activity compared to its mutant and deletion mutant counterparts (Figure 2B). The polypeptide p196, driven by the IRES, shares an identical sequence with the 101–289aa region of FOXP1 and is recognized by antibodies targeting the common sequence "QMQQLQQQHLLSLQRQGLLTIQPGQPALPLQPLAQGMIPTELQQLWKEVTSAHTAEETTGNNHSSLDLTTT-CVSSSAPSKTSLIMNPHASTNGQLSVHTPKRE" (Figure 2C). Notably, significantly higher expression of p196 was observed in HCC cell lines compared to normal liver cell lines (Figure 2D).

To validate the encoding of p196 by circFOXP1, we constructed several plasmids: circFOXP1 with an IRES mutation (circFOXP1 IRES-mut), circFOXP1 overexpression plasmid, linearized p196 overexpression plasmid, and junction-specific shRNAs targeting circFOXP1. Transfection with both circFOXP1 and linearized p196 plasmids led to
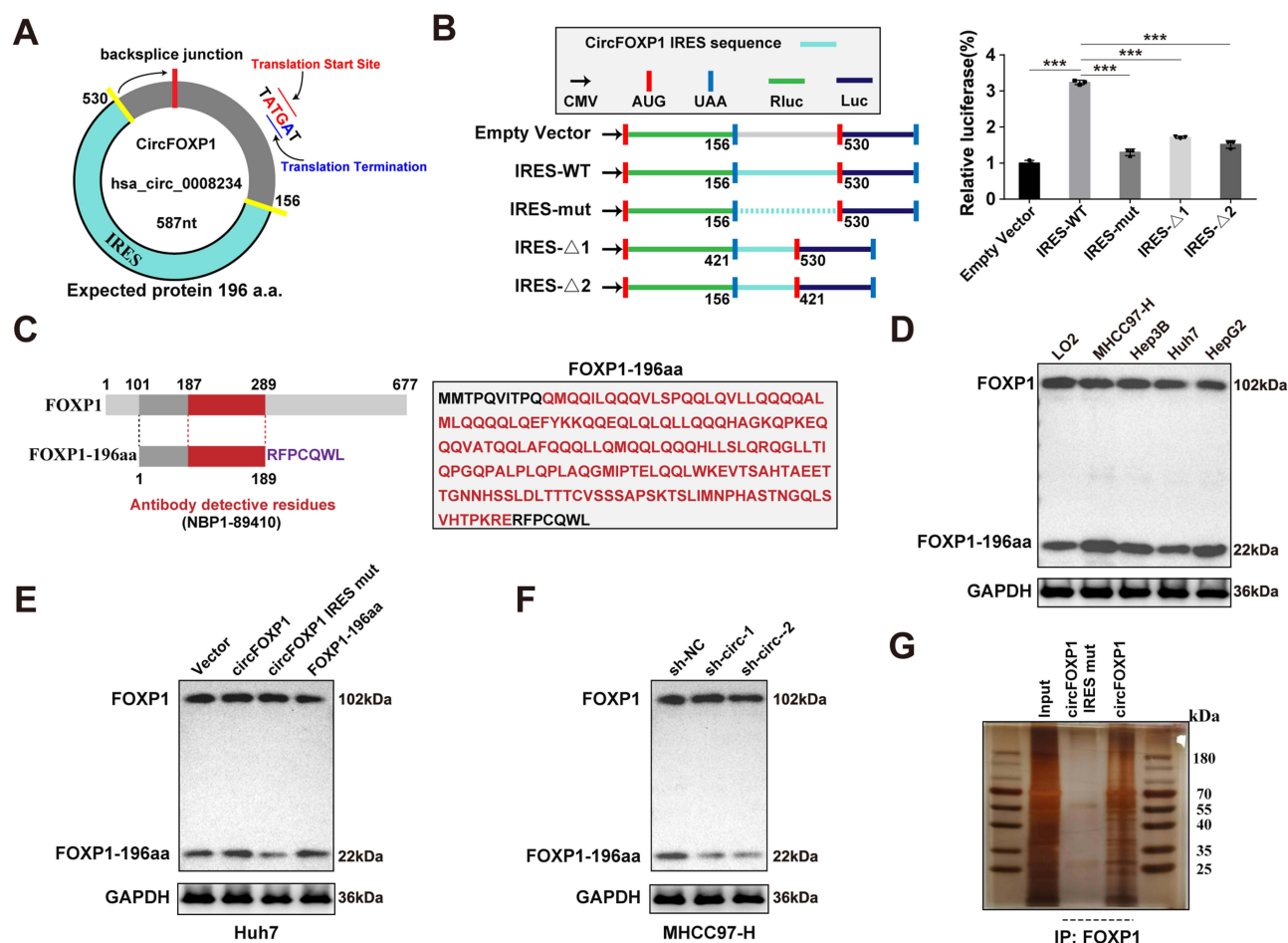
Figure 2 circFOXP1 encodes a novel protein p196 with 196 amino acids (aa). (**A**) Schematic diagram shows that circFOXP1 has an internal ribosome entry site (IRES) and a predicted open reading frame, which may encode a 196 amino acid (aa) polypeptide. (**B**) Dual luciferase assay shows that the Luc/Rluc activity of the wild-type IRES is higher than that of its mutant and deletion mutant. (**C**) Sequence diagram of p196 and FOXP1 recognizable by antibodies. (**D**) Western blot (WB) analysis shows that p196 is highly expressed in HCC cells. (**E**) HCC cells were transfected with empty vector, circFOXP1 vector, circFOXP1 IRES mutant vector, and linearized FOXP1-196aa vector, respectively. The levels of FOXP1 and p196 were detected by WB. (**F**) HCC cells were transfected with junction-specific shRNA targeting circFOXP1. The levels of FOXP1 and p196 were detected by WB. (**G**) Silver staining shows that p196 is within the predicted molecular weight range. ***P<0.001.

a significant increase in p196 expression, whereas the circFOXP1 IRES-Mut plasmid did not exhibit such an effect (Figure 2E). Conversely, shRNAs specific to circFOXP1 reduced p196 levels without altering FOXP1 protein expression (Figure 2F). Silver staining confirmed the predicted molecular weight of p196 (Figure 2G), and both mass spectrometry analysis and SDS-PAGE validated its sequence (Figure S2A). Collectively, these findings provide evidence that p196 is encoded by circFOXP1.

p196, Rather Than circFOXP1, Promotes the Growth and Invasiveness of HCC Cells

To explore the biological roles of p196 in HCC progression, we established Huh7 and MHCC97-H cell lines over-expressing p196 using linearized FOXP1-196aa and circFOXP1 plasmids. Additionally, we generated stable p196 knockdown cell lines in both Huh7 and MHCC97-H using shRNA with specific targeting. Our findings revealed that the proliferation and invasion capabilities of HCC cell lines overexpressing p196, achieved through both linearized FOXP1-196aa and circFOXP1 plasmids, were markedly increased. This enhancement was more evident in cell lines established with linearized FOXP1-196aa plasmids, while p196 knockdown led to opposite effects (Figure 3A–H). Western blotting experiments further disclosed that HCC cells transfected with either linearized FOXP1-196aa or circFOXP1 plasmids exhibited significantly upregulated expression of key cell cycle regulatory proteins (cyclin D1, CDK4). Similarly, the expression levels of epithelial-mesenchymal transition (EMT)-associated proteins (N-cadherin and Vimentin) were elevated, whereas E-cadherin expression was decreased; conversely, their deletion resulted in opposite effects (Figure 3I and J). These observations suggest that p196 substantially promotes the growth and invasion of HCC cells.

To demonstrate that p196, rather than circFOXP1, is involved in HCC progression, we restored p196 expression in HCC cells with stable p196 knockdown by transfecting them with linearized FOXP1-196aa plasmids. Notably, the restoration of p196 reversed the inhibitory effects of circFOXP1 knockdown on the malignant phenotype of HCC (Figure 3B, D, F, H, J). Although the IRES-mutated circFOXP1 plasmid cannot translate p196 in vivo, its altered structure may exert potential functional effects. Therefore, we further assessed the influence of IRES-mutated circFOXP1 on the proliferation and invasion abilities of HCC cells. The results indicated that the circFOXP1 ATG mutant plasmid did not enhance the malignant phenotype of HCC cells (Figure S2B–F). These findings confirm that p196, rather than circFOXP1, exerts oncogenic effects.

## circFOXP1 Promotes HCC Progression Through Autophagy-Related Pathways

To elucidate the key biological pathways influenced by circFOXP1, we conducted a GSEA analysis, which revealed a significant enrichment of autophagy-related pathways in HCC (Figure 4A and B). Utilizing Western blotting, we assayed the autophagy markers LC3-I and LC3-II and discovered that the upregulation of circFOXP1 led to an enhancement in the expression level of LC3-II, whereas downregulation resulted in the opposite effect (Figure 4C). Notably, the elevated expression of LC3-II due to circFOXP1 overexpression could be reversed by treatment with 3-MA, an autophagy inhibitor that obstructs autophagosome formation (Figure 4D). Consistent with autophagy flux, observations from the mCherry-GFP-LC3 reporter gene assay and transmission electron microscopy corroborated that circFOXP1 substantially increased the number of autophagic vacuoles in both Huh7 and MHCC97-H cells (Figure 4E and F). In summary, our findings suggest that circFOXP1 can stimulate autophagy in HCC cells.

Subsequently, we examined whether the oncogenic effects of circFOXP1 were impacted by the autophagy inhibitor 3-MA. As anticipated, the overexpression of circFOXP1 augmented the proliferation and invasion of Huh7 and MHCC97-H cells, and these effects were reversed by 3-MA treatment (Figure 4G–J). Collectively, these data provide evidence that circFOXP1 promotes the progression of HCC by enhancing autophagy.

p196 Regulates the Proliferation and Invasion of Liver Cancer Mediated by Autophagy Through ULK1

To explore the potential mechanisms underlying the cancer-promoting effect of circFOXP1, we first investigated whether circFOXP1 functions as a miRNA sponge. Argonaute 2 (Ago2) crosslinking and immunoprecipitation assays revealed that
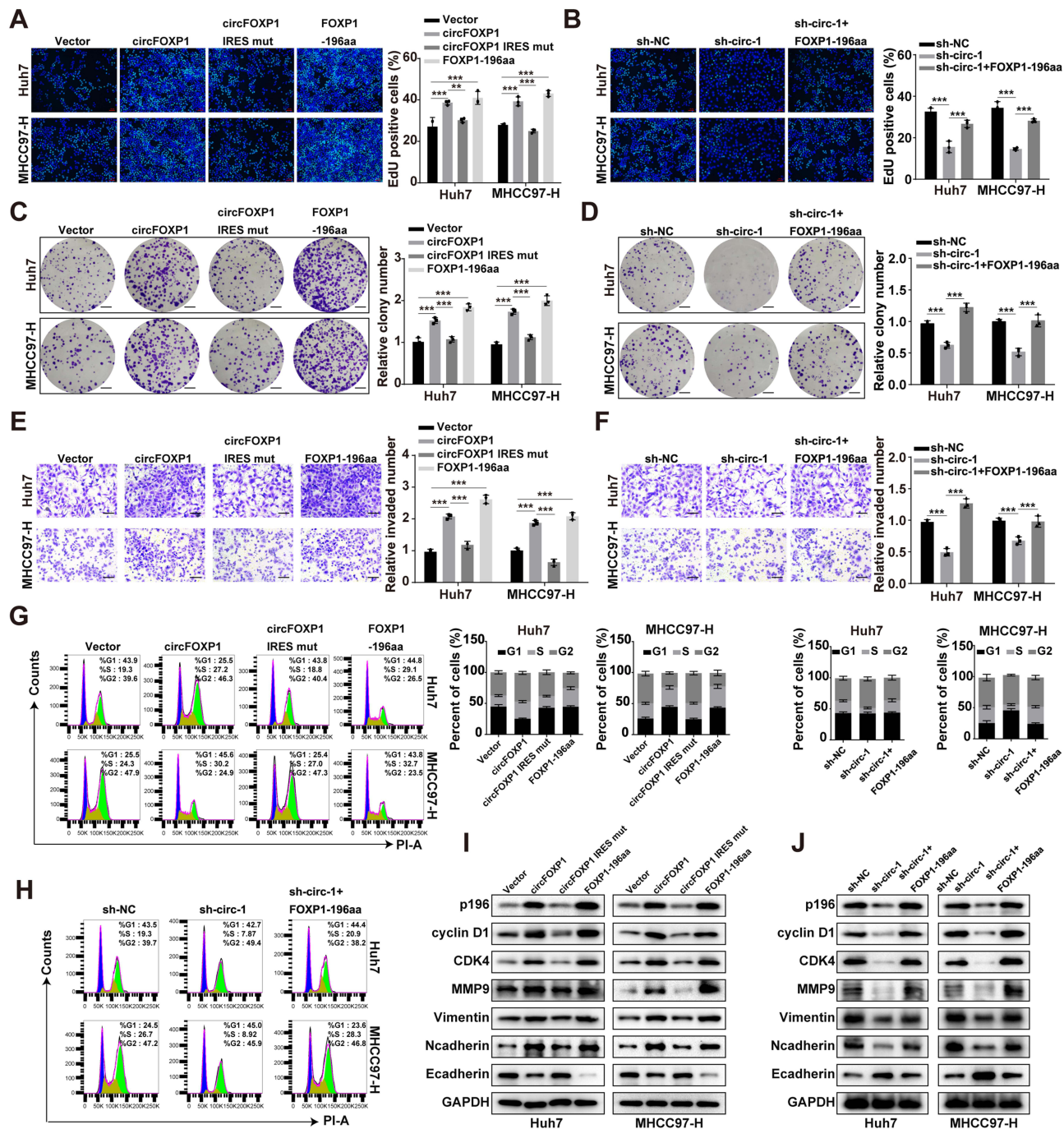
Figure 3 P196 promotes proliferation and invasiveness of HCC cells. (**A–D**) P196-overexpressing Huh7 and MHCC97-H cell lines were established by transfection with linearized FOXP1-196aa plasmid and circFOXP1 plasmid. P196 stably knockdown Huh7 and MHCC97-H cell lines were established by connecting specific shRNA. The expression level of P196 in stably knockdown HCC cells was restored using linearized FOXP1-196aa plasmid. The proliferation of HCC cells was detected using the Edu assay (scale: 100 μm) (**A** and **B**) and colony formation assay (**C** and **D**). (**E** and **F**) The invasion ability of HCC cells was detected using the matrix invasion assay. Scale: 100 μm. (**G** and **H**). The effect of P196 on the cell cycle of HCC cells was detected by flow cytometry. (**I** and **J**) WB analysis of the expression levels of cell cycle regulatory proteins and EMT-related proteins. **P<0.01, and ***P<0.001.

circFOXP1 does not bind to Ago2, ruling out the possibility that circFOXP1 exerts its effects through the competing endogenous RNA (ceRNA) network mechanism (Figure 5A). Given that ULK1 exhibits the most prominent expression in the autophagy pathway (Figure S3), we formulated the hypothesis that p196 regulates autophagy and, consequently, modulates the biological effects of liver cancer via ULK1. Employing qRT-PCR and Western blotting, we observed that overexpression of p196 led to increased mRNA and protein levels of ULK1 in Huh7 and MHCC97-H cells, whereas knockdown of p196 produced
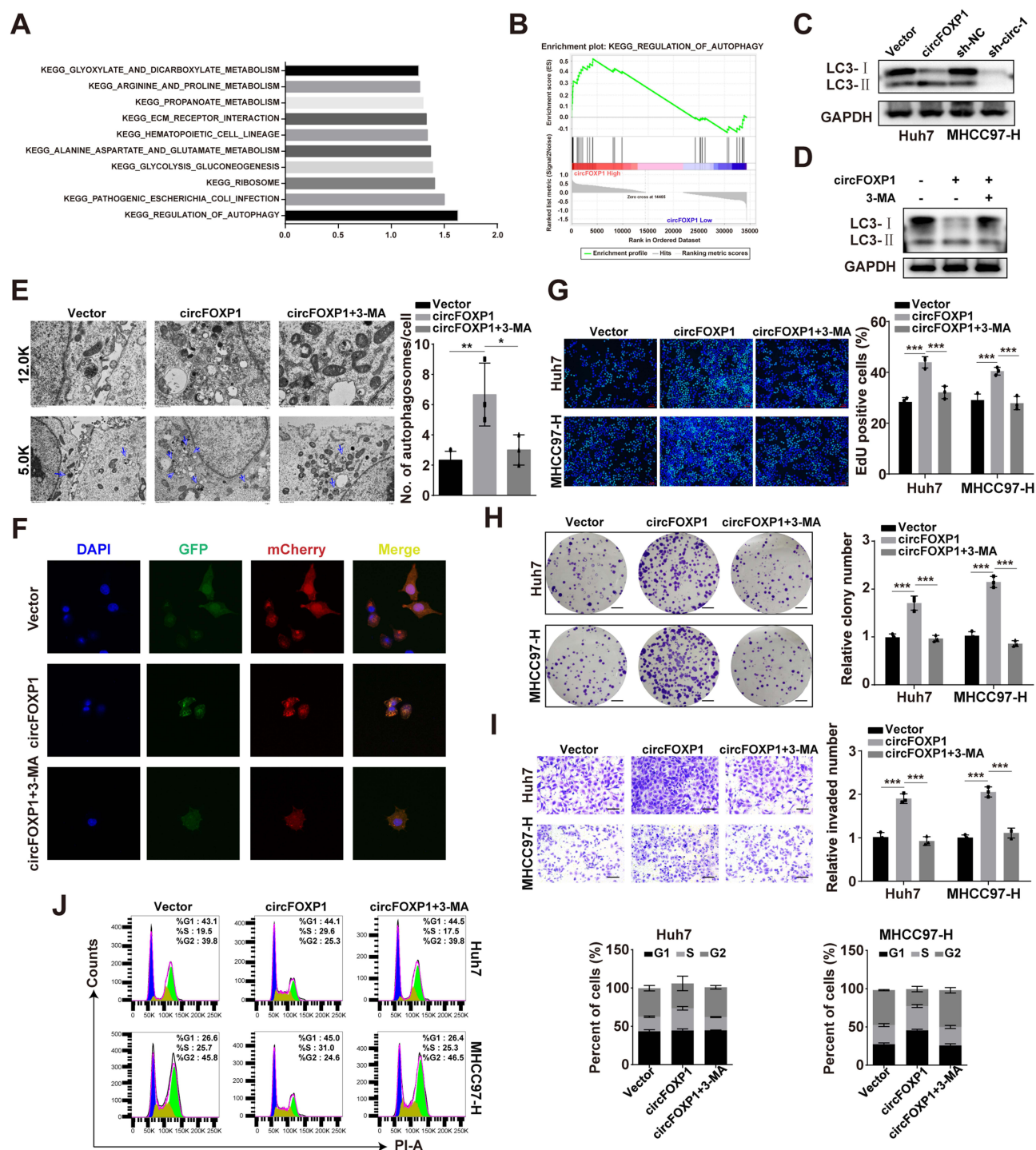
Figure 4 circFOXP1 promotes HCC progression through autophagy-related pathways. (**A**) Gene set enrichment analysis (GSEA) reveals the top 10 pathways associated with high expression of circFOXP1. (**B**) GSEA plot shows a positive correlation between circFOXP1 expression and a set of genes upregulated in autophagy-related pathways in liver cancer. (**C** and **D**). Western blotting analysis of LC3II/I protein levels in HCC cells. (**E**) Observation of autophagosomes by electron microscopy. (**F**) Immunofluorescence staining of autophagosomes and autolysosomes. (**G** and **H**). Detection of proliferation of HCC cells using the Edu method (scale: 100 μm) (**G**) and colony formation assay (**H**). (**I**) Detection of invasion ability of HCC cells using the matrix invasion assay. Scale: 100 μm. (**J**). Flow cytometry analysis of the cell cycle of HCC cells. *P<0.05, **P<0.01, ***P<0.001.

the opposite effects (Figure 5B and C). Subsequently, we transfected HCC cells with either sh-ULK1 alone or in combination with the circFOXP1 overexpression vector. Initially, transfection with sh-ULK1 effectively diminished ULK1 protein levels in Huh7 and MHCC97-H cells (Figure 5D). We then discovered that the elevated LC3-II expression levels induced by circFOXP1 overexpression could be reversed by sh-ULK1 (Figure 5E). After that, we assessed whether the oncogenic effects of circFOXP1
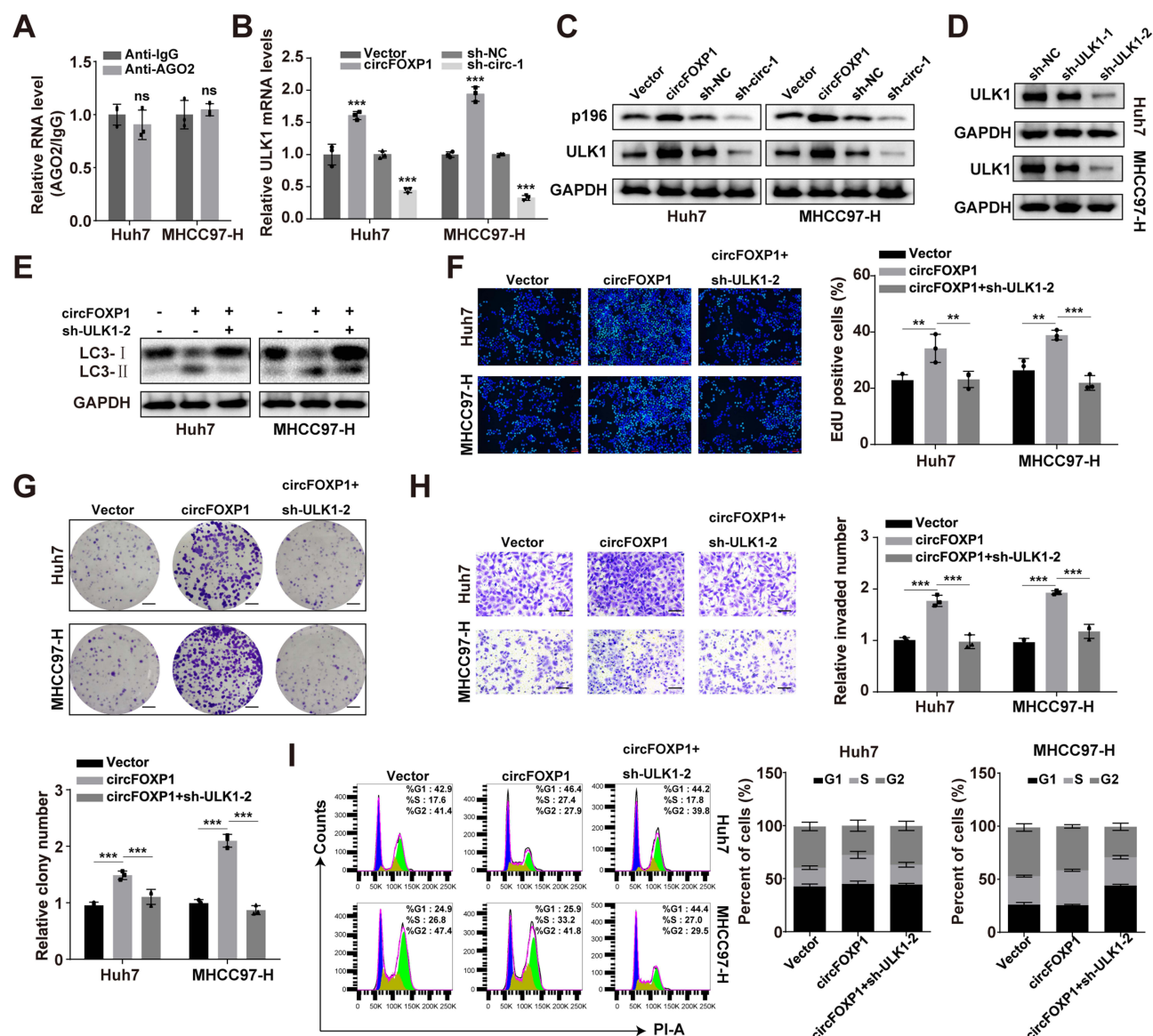
Figure 5 P196 regulates the proliferation and invasion of liver cancer mediated by autophagy through ULK1. (**A**) RNA immunoprecipitation (RIP) assay validates the interaction between circFOXP1 and Ago2. (**B**). qRT-PCR analysis of ULK1 mRNA in HCC stably transfected with Vector, circFOXP1, and sh-circFOXP1. (**C**) WB analysis of p196 and ULK1 expression in HCC cells with p196 knockdown and overexpression. (**D**) Western blot analysis of ULK1 expression in HCC transfected with sh-ULK1-1, sh-ULK1-2, and sh-NC lentiviruses. (**E**) WB experiments showed that sh-ULK1-2 could reverse the positive effect of p196 on LC3II/I in HCC cells. (**F** and **G**). Huh7 and MHCC97-H cell lines were transfected with circFOXP1 plasmid and/or sh-ULK1-2, and the proliferation of HCC cells was detected using the Edu method (scale: 100 μm) (**E**) and colony formation method (**F**). (**H**). The invasion ability of HCC cells was detected using the matrix invasion method. Scale: 100 μm. (**I**). Flow cytometry was used to detect the effect of P196 on the cell cycle of HCC cells. **$P<0.01$, ***$P<0.001$.

were influenced by ULK1. As anticipated, circFOXP1 overexpression augmented the proliferation and invasion of Huh7 and MHCC97-H cells, and these effects could be reversed by knockdown of ULK1 (Figure 5F and G). Collectively, these findings suggest that p196 promotes the progression of HCC by modulating autophagy through ULK1.

The Interaction Between p196 and KHDRBS3 Stabilizes ULK1 mRNA

Numerous studies have established the pivotal role of ULK1 mRNA stability in the autophagy process.[24–26] Building on this foundation, we postulate that p196 exerts its functional effects by modulating ULK1 mRNA stability. Specifically, overexpression, knockdown, or manipulation of circFOXP1 leads to significant increases or decreases in the half-life of ULK1 mRNA in Huh7 and MHCC97-H cells (Figure 6A–B). RNA immunoprecipitation (RIP) experiments have demonstrated that p196 can enrich ULK1 mRNA (Figure 6C). To investigate the RNA-binding proteins (RBPs) involved
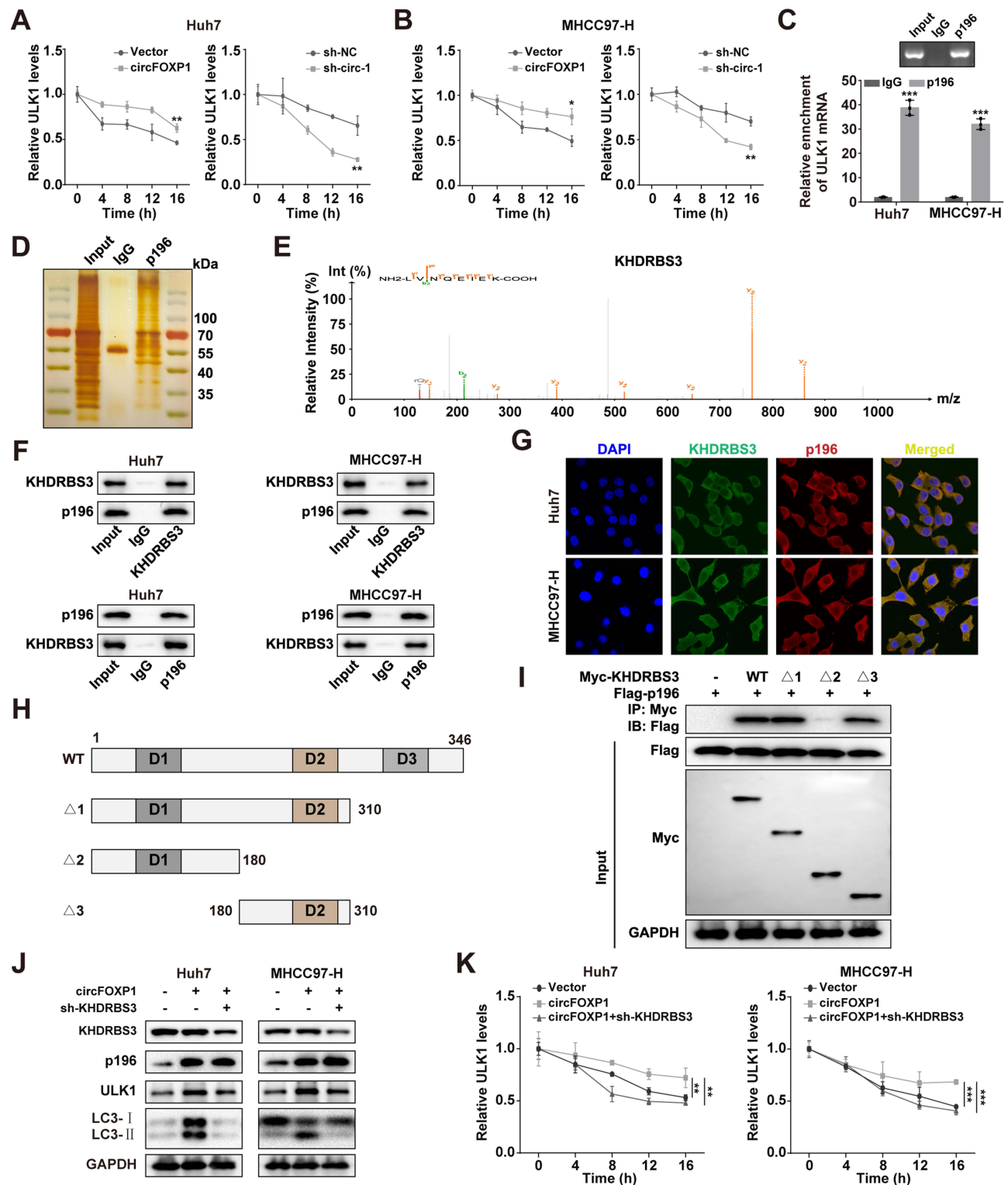
Figure 6 The interaction between p196 and KHDRBS3 stabilizes ULK1 mRNA. (**A** and **B**) HCC cells with p196 knockdown and overexpression were treated with 2 μg/mL actinomycin at specified time points, followed by qRT-PCR to detect the relative expression of ULK1 mRNA. (**C**) RNA immunoprecipitation experiments indicated that p196 could bind to ULK1 mRNA. (**D**) Silver Staining assay showed that proteins co-precipitated by p196 from Huh7 cell lysates identified a specific band at 55 kDa. (**E**). Mass spectrometry analysis detected a peptide of KHDRBS3 (n = 1 for both IgG and p196 groups), indicating an interaction between p196 and KHDRBS3. (**F**). Co-immunoprecipitation experiments demonstrated the interaction between p196 and KHDRBS3. (**G**) IF detection showed the co-localization of p196 (red) and KHDRBS3 (green) in liver cancer cells. Scale: 10 μm. (**H**). Schematic diagram of KHDRBS3 truncated domains. (**I**). In vitro binding experiments revealed the specific region of p196 that binds to KHDRBS3. (**J**) WB experiments indicated that sh-KHDRBS3 could reverse the positive effect of p196 on LC3II/I and ULK1 in liver cancer cells. (**K**) KHDRBS3 was knocked down in HCC cells with p196 overexpression, followed by treatment with 2 μg/mL actinomycin at specified time points, and then qRT-PCR was used to detect the relative expression of ULK1. *P<0.05, **P<0.01, ***P<0.001.

in the regulation of ULK1 mRNA stability by p196, we conducted Silver Staining assays. The results revealed a distinct band at 55 kDa (Figure 6D). Subsequent mass spectrometry analysis of proteins co-precipitated with p196 and IgG identified KHDRBS3 as the most abundant interactor among the differentially expressed proteins between the p196 and IgG groups (Figure 6E). The interaction between endogenous p196 and KHDRBS3 was confirmed through co-immunoprecipitation (co-IP) experiments (Figure 6F). Additionally, immunofluorescence (IF) experiments showed that p196 colocalizes with KHDRBS3 in the cytoplasm (Figure 6G). To delineate the domains necessary for the interaction between p196 and KHDRBS3, we generated various deletion mutants of Flag-p196 and Myc-KHDRBS3 in Huh7 cells. Co-IP experiments verified that the D2 domain of KHDRBS3 (amino acids 180–310) specifically binds to p196 (Figure 6H–I). Furthermore, we observed that knockdown of KHDRBS3 significantly reversed the increase in ULK1 protein levels induced by p196 overexpression (Figure 6J). Similarly, knockdown of KHDRBS3 also abrogated the enhancement of ULK1 mRNA stability by p196 overexpression (Figure 6K). In conclusion, p196 interacts with KHDRBS3 to stabilize ULK1 mRNA.
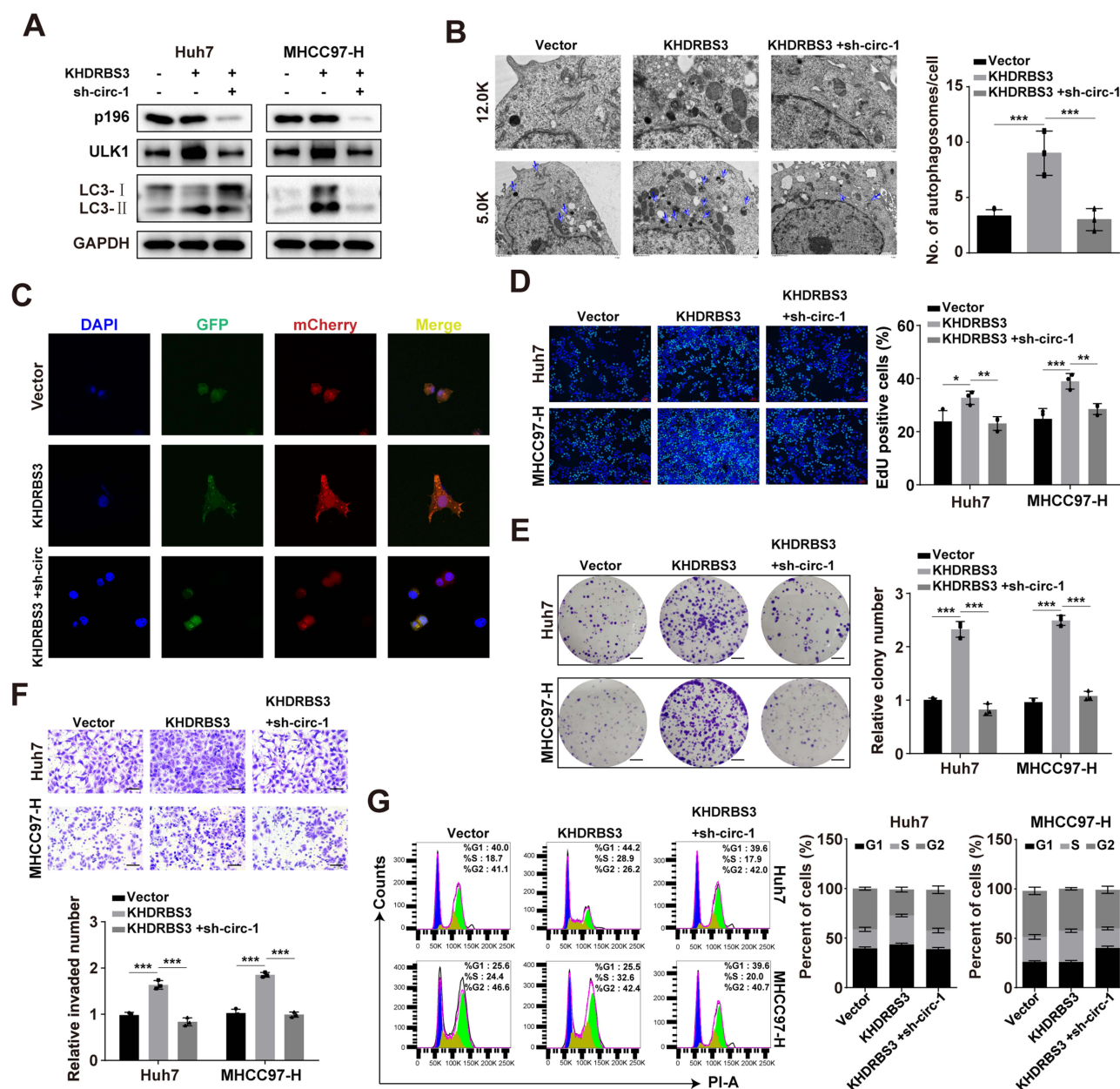
p196 Acts as a Scaffold to Promote KHDRBS3 Binding to ULK1, Enhancing Autophagy and Liver Cancer Progression

Considering the regulatory roles of both p196 and KHDRBS3 on ULK1 expression and their mutual binding interaction, we postulate that p196 serves as a scaffold to facilitate the binding of KHDRBS3 to ULK1. Consistent with our hypothesis, Western blot analysis demonstrated that knockdown of p196 reversed the KHDRBS3-induced upregulation of ULK1 expression (Figure 7A). To further examine whether KHDRBS3 promotes autophagy and the progression of hepatocellular carcinoma (HCC) cells in a p196-dependent manner, we employed KHDRBS3 overexpression vectors in combination with or without sh-circFOXP1 vectors. The elevated LC3-II levels resulting from KHDRBS3 overexpression were abrogated by sh-circFOXP1 (Figure 7A). The findings from the mCherry-GFP-LC3 reporter gene assay were corroborated by transmission electron microscopy analysis (Figure 7B and C). Moreover, KHDRBS3 significantly augmented the proliferation and invasion capabilities of HCC cells, which were reversible upon knockdown of p196 (Figure 7D–G). In conclusion, KHDRBS3 enhances autophagy levels and promotes the onset and progression of liver cancer in a manner dependent on p196.

Exosomal circFOXP1 from HCC Cells Enhances Cancer Cell Progression

Recent studies have indicated that exosomes are the primary carriers of extracellular circular RNAs (circRNAs), which can be transmitted through exosomes and play a critical role in intercellular communication.[8,33–36] In this context, we explored whether extracellular circFOXP1 can influence HCC progression via exosome-mediated transfer. Initially, we observed that after treatment with RNase A, the levels of circFOXP1 in the culture medium were almost equal to those in the control group. However, when RNase A was combined with Triton-100 treatment, the expression level of circFOXP1 in the HCC cell culture medium significantly decreased (Figure 8A), suggesting that circFOXP1 is predominantly transferred via exosomes rather than being directly released. Exosomes were isolated from MIHA, Huh7, and MHCC97-H cells, and the presence of exosomes in these culture media was confirmed by transmission electron microscopy (TEM) (Figure 8B). Nanoparticle tracking analysis (NTA) revealed the quantity and size distribution of the exosomes (Figure 8C). Western blot analysis showed that the exosomes isolated from HCC cells were enriched in exosomal markers HSP70, TSG101, CD63, and CD9 (Figure 8D). qRT-PCR results indicated that the expression levels of circFOXP1 in the culture medium were not significantly different from those in the exosomes (Figure 8E), confirming that exosomes are the main carriers of extracellular circFOXP1. Furthermore, qRT-PCR results demonstrated that the expression of exosomal circFOXP1 was lowest in MIHA cells and relatively higher in HCC cells (Figure 8F). After co-culturing with exosomes derived from MHCC97-H cells, the expression of circFOXP1 in recipient Huh7 cells increased significantly, whereas co-culturing with exosomes from circFOXP1 knockdown MHCC97-H cells showed the opposite result (Figure 8G). To investigate whether exosomal circFOXP1 could be taken up by recipient cells, we co-cultured exosomes isolated from MHCC97-H (CD63-Cre) cells with Huh7 (LoxP-DsRed-Stop-LoxP-GFP) cells. Fluorescence

Figure 7 P196 acts as a scaffold to promote KHDRBS3 binding to ULK1, enhancing autophagy and liver cancer progression. (**A**) Western blot (WB) experiments showed that knockdown of p196 could reverse the positive effect of KHDRBS3 on ULK1 and LC3II/I in HCC cells. (**B**) Observation of autophagosomes by electron microscopy. (**C**) Immunofluorescence staining of autophagosomes and autolysosomes. (**D** and **E**) Detection of proliferation of HCC cells using the EdU method (scale: 100 μm) (**D**) and colony formation assay (**E**). (**F**) Detection of invasion ability of HCC cells using the matrix invasion assay. Scale: 100 μm. (**G**). Flow cytometry analysis of the cell cycle of HCC cells. *P<0.05, **P<0.01, ***P<0.001.

microscopy revealed that some Huh7 cells had taken up the exosomes, with red signals converting to green signals (Figure 8H and I).

To further confirm the decisive role of exosomal circFOXP1 in HCC cell progression, we first pretreated MHCC97-H cells with GW4869 to inhibit exosome production (Figure S4A and B). Subsequently, we isolated exosomes from MHCC97-H cells transfected with Vector/circFOXP1 constructs and found that co-incubation with circFOXP1-EXO significantly enhanced the proliferation, invasion, and cell cycle progression of HCC cells, an effect that could be rescued by GW4869 treatment (Figure S4C–F). In summary, exosomal circFOXP1 from HCC cells enhances the progression of cancer cells.
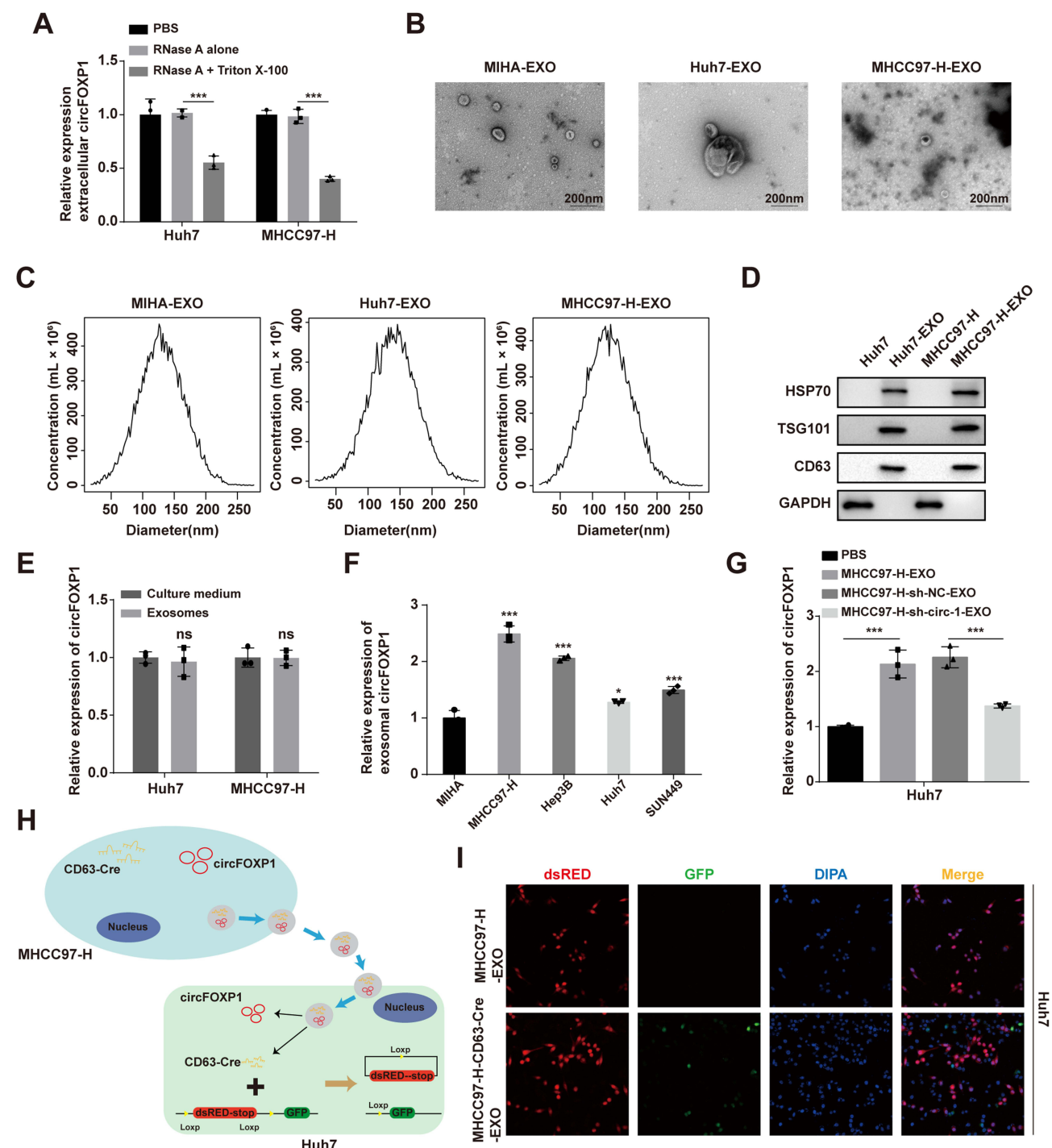
Figure 8 Exosomes are the primary carriers of extracellular circFOXP1. (**A**) qRT-PCR analysis of circFOXP1 expression in the HCC cell culture medium treated with PBS, RNase A alone, or RNase A in combination with Triton X-100. (**B**) Transmission electron microscopy images showing the morphology of exosomes isolated from the supernatants of MIHA, Huh7, and MHCC97-H cultures. (**C**) NTA analysis displays the quantity and size distribution of exosomes isolated from the supernatants of MIHA, Huh7, and MHCC97-H cultures. (**D**) Western blot analysis demonstrating the expression of exosomal markers in the exosomes isolated from the supernatants of Huh7 and MHCC97-H cultures. (**E**) qRT-PCR analysis shows the relative expression of circFOXP1 in exosomes and cell culture medium. (**F**) qRT-PCR analysis displaying the relative expression of circFOXP1 in exosomes from different cell lines. (**G**) qRT-PCR analysis indicates the expression of circFOXP1 after co-culturing exosomes isolated from Huh7 and MHCC97-H cells stably transfected with sh-NC (negative control short hairpin RNA) or sh-circFOXP1 (short hairpin RNA targeting circFOXP1). (**H**) Schematic illustration of the uptake of exosomes secreted by MHCC97-H cells by Huh7. (**I**) Immunofluorescence analysis showing changes in fluorescence after Huh7 uptake of exosomes secreted by MHCC97-H cells. Scale: 20X. * p < 0.05, *** p < 0.001, ns, not significant.

Discussion

The findings presented in this study represent a significant advancement in our understanding of the role of circular RNAs (circRNAs) in the progression of liver cancer. We discovered that circFOXP1 can be transmitted intercellularly via exosomes and identified a novel 196-amino acid protein, termed p196, encoded by circFOXP1. This revelation unveils a previously unrecognized mechanism through which circRNAs can exert a direct influence on tumorigenesis. This discovery not only highlights the functional versatility of circRNAs but also opens up new avenues for the development of targeted therapies for liver cancer.

The core significance of this study resides in its demonstration that circFOXP1, a tumor-promoting circRNA previously associated with liver cancer, encodes a functional protein, p196, which actively fosters cancer cell growth and invasion. By conducting a series of meticulously designed experiments, we have elucidated that p196 interacts with KHDRBS3 to stabilize ULK1 mRNA, resulting in heightened levels of autophagy and accelerated cancer progression. This mechanistic understanding offers a novel rationale for the oncogenic effects exerted by circFOXP1 and emphasizes the crucial importance of exploring circRNA-encoded proteins within the realm of cancer biology.

Our findings further underscore the pivotal role of autophagy in the progression of liver cancer, aligning with earlier studies that have implicated autophagy in both the suppression and promotion of tumors.[6,37] By elucidating that p196 modulates autophagy via ULK1, we contribute to the expanding evidence base highlighting autophagy as a fundamental regulator of cancer cell behavior and a prospective therapeutic target.

Although our study presents compelling evidence supporting the oncogenic function of p196 in liver cancer, several limitations must be recognized. Firstly, our functional validation was conducted primarily using in vitro and xenograft mouse models. To fortify our findings and gain deeper insights into the in vivo relevance of p196, future studies utilizing genetically engineered mouse models that emulate the development of human liver cancer would be invaluable. Secondly, the clinical implications of p196 expression in human liver cancer patients have yet to be comprehensively elucidated. Conducting large-scale cohort studies to correlate p196 expression with patient outcomes would yield invaluable information regarding its prognostic significance and potential utility as a biomarker for disease progression. Furthermore, our study exclusively focused on the role of p196 in autophagy regulation. Given the pleiotropic nature of circRNAs and their encoded proteins, further exploration into additional biological functions of p196, such as its impact on metabolic reprogramming or immune evasion, may reveal additional mechanisms underlying liver cancer progression.

The identification of p196 as a tumor-promoting protein encoded by circFOXP1 in liver cancer raises the possibility that similar mechanisms may operate in other tumor types. Recent studies have demonstrated the functional importance of circRNAs and their encoded proteins in a variety of malignancies.[38–40] For example, circMTHFD2L-encoded peptides have been shown to promote breast cancer progression,[41] while the expression of circFAM53B and its encoded peptide is associated with extensive infiltration of antigen-specific CD8+ T cells and better survival in breast cancer and melanoma patients.[42] These findings suggest that the exploration of circRNA-encoded proteins across different tumor types may reveal shared oncogenic pathways and identify novel therapeutic targets.

Future research endeavors ought to concentrate on deciphering the clinical pertinence of p196 expression in liver cancer patients, as well as exploring additional biological roles of p196 that extend beyond its regulation of autophagy. Additionally, the development of targeted inhibitors against p196 or its interacting partners, such as KHDRBS3, may present novel therapeutic avenues for the treatment of liver cancer.

Conclusion

In summary, our study reveals a novel mechanism by which exosome-delivered circFOXP1 promotes the progression of liver cancer through the encoding of the p196 protein. By elucidating the interaction between p196 and KHDRBS3, which stabilizes ULK1 mRNA and enhances autophagy, we provide significant insights into the functional importance of circular RNA-encoded proteins in cancer. These findings have substantial implications for our understanding of liver cancer biology and may pave the way for the development of innovative therapeutic strategies to combat this life-threatening disease.

Data Sharing Statement

The datasets used and/or analyzed during the current study are available from the corresponding author on reasonable request.

 5263

Ethics Approval and Consent to Participate

The study was approved by the ethics committee of the Huazhong University of Science and Technology, and all included patients provided written informed consent. All methods were carried out in accordance with relevant guidelines and regulations. All animal experiments were carried out according to the guidelines and experiments were approved by the Institutional Animal Care Use Committee of Huazhong University of Science and Technology.

Acknowledgments

Author Contributions

All authors made a significant contribution to the work reported, whether that is in the conception, study design, execution, acquisition of data, analysis, and interpretation, or all these areas; took part in drafting, revising, or critically reviewing the article; gave final approval of the version to be published; have agreed on the journal to which the article has been submitted; and agree to be accountable for all aspects of the work.

Funding

Disclosure

The authors declare that they have no competing interests.

References

1. Balogh J, Victor III D, Asham EH, Burroughs SG, et al. Hepatocellular carcinoma. *Nat Rev Dis Primers*. 2021;7(1):7. doi:10.1038/s41572-021-00245-6
2. Sung H, Ferlay J, Siegel RL, et al. Global Cancer Statistics 2020: GLOBOCAN Estimates of Incidence and Mortality Worldwide for 36 Cancers in 185 Countries. *CA Cancer J Clin*. 2021;71(3):209–249. doi:10.3322/caac.21660
3. Nagaraju GP, Dariya B, Kasa P, Peela S, El-Rayes BF. Epigenetics in hepatocellular carcinoma. *Semin Cancer Biol*. 2022;86(Pt 3):622–632. doi:10.1016/j.semcancer.2021.07.017
4. Finn RS, Qin S, Ikeda M, et al. Atezolizumab plus Bevacizumab in Unresectable Hepatocellular Carcinoma. *N Engl J Med*. 2020;382 (20):1894–1905. doi:10.1056/NEJMoa1915745
5. Patop IL, Wust S, Kadener S. Past, present, and future of circRNAs. *EMBO J*. 2019;38(16):e100836. doi:10.15252/embj.2018100836
6. Levy JMM, Towers CG, Thorburn A. Targeting autophagy in cancer. *Nat Rev Cancer*. 2017;17(9):528–542. doi:10.1038/nrc.2017.53
7. Chen L, Shan G. CircRNA in cancer: fundamental mechanism and clinical potential. *Cancer Lett*. 2021;505:49–57. doi:10.1016/j.canlet.2021.02.004
8. Hu Z, Chen G, Zhao Y, et al. Exosome-derived circCCAR1 promotes CD8 + T-cell dysfunction and anti-PD1 resistance in hepatocellular carcinoma. *mol Cancer*. 2023;22(1):55. doi:10.1186/s12943-023-01759-1
9. Liu B, Shen H, He J, et al. Cytoskeleton remodeling mediated by circRNA-YBX1 phase separation suppresses the metastasis of liver cancer. *Proc Natl Acad Sci U S A*. 2023;120(30):e2220296120. doi:10.1073/pnas.2220296120
10. Xu L, Wang P, Li L, et al. circPSD3 is a promising inhibitor of uPA system to inhibit vascular invasion and metastasis in hepatocellular carcinoma. *mol Cancer*. 2023;22(1):174. doi:10.1186/s12943-023-01882-z
11. Pegtel DM, Gould SJ. Exosomes. *Annu Rev Biochem*. 2019;88(1):487–514. doi:10.1146/annurev-biochem-013118-111902
12. Salunkhe S, Basak M, Chitkara D, Mittal A, Mittal A. Surface functionalization of exosomes for target-specific delivery and in vivo imaging & tracking: strategies and significance. *J Control Release*. 2020;326:599–614. doi:10.1016/j.jconrel.2020.07.042
13. Liang Y, Duan L, Lu J, Xia J. Engineering exosomes for targeted drug delivery. *Theranostics*. 2021;11(7):3183–3195. doi:10.7150/thno.52570
14. Kimiz-Gebologlu I, Oncel SS. Exosomes: large-scale production, isolation, drug loading efficiency, and biodistribution and uptake. *J Control Release*. 2022;347:533–543. doi:10.1016/j.jconrel.2022.05.027
15. Dai J, Su Y, Zhong S, et al. Exosomes: key players in cancer and potential therapeutic strategy. *Signal Transduct Target Ther*. 2020;5(1):145. doi:10.1038/s41392-020-00261-0
16. Xu Z, Chen Y, Ma L, et al. Role of exosomal non-coding RNAs from tumor cells and tumor-associated macrophages in the tumor microenvironment. *Mol Ther*. 2022;30(10):3133–3154. doi:10.1016/j.ymthe.2022.01.046
17. Li C, Ni YQ, Xu H, et al. Roles and mechanisms of exosomal non-coding RNAs in human health and diseases. *Signal Transduct Target Ther*. 2021;6(1):383. doi:10.1038/s41392-021-00779-x

18. Zhang Y, Jiang J, Zhang J, et al. CircDIDO1 inhibits gastric cancer progression by encoding a novel DIDO1-529aa protein and regulating PRDX2 protein stability. *mol Cancer*. 2021;20(1):101. doi:10.1186/s12943-021-01390-y

19. Liu H, Fang D, Zhang C, et al. Circular MTHFD2L RNA-encoded CM-248aa inhibits gastric cancer progression by targeting the SET-PP2A interaction. *Mol Ther*. 2023;31(6):1739–1755. doi:10.1016/j.ymthe.2023.04.013

20. Song R, Ma S, Xu J, et al. A novel polypeptide encoded by the circular RNA ZKSCAN1 suppresses HCC via degradation of mTOR. *mol Cancer*. 2023;22(1):16. doi:10.1186/s12943-023-01719-9

21. Mizushima N, Yoshimori T, Ohsumi Y. The role of Atg proteins in autophagosome formation. *Annu Rev Cell Dev Biol*. 2011;27(1):107–132. doi:10.1146/annurev-cellbio-092910-154005

22. Rogov V, Dotsch V, Johansen T, Kirkin V. Interactions between autophagy receptors and ubiquitin-like proteins form the molecular basis for selective autophagy. *Mol Cell*. 2014;53(2):167–178. doi:10.1016/j.molcel.2013.12.014

23. Umemura A, He F, Taniguchi K, et al. p62, Upregulated during Preneoplasia, Induces Hepatocellular Carcinogenesis by Maintaining Survival of Stressed HCC-Initiating Cells. *Cancer Cell*. 2016;29(6):935–948. doi:10.1016/j.ccell.2016.04.006

24. Deng G, Zeng S, Qu Y, et al. BMP4 promotes hepatocellular carcinoma proliferation by autophagy activation through JNK1-mediated Bcl-2 phosphorylation. *J Exp Clin Cancer Res*. 2018;37(1):156. doi:10.1186/s13046-018-0828-x

25. Fan Q, Yang L, Zhang X, et al. Autophagy promotes metastasis and glycolysis by upregulating MCT1 expression and Wnt/beta-catenin signaling pathway activation in hepatocellular carcinoma cells. *J Exp Clin Cancer Res*. 2018;37(1):9. doi:10.1186/s13046-018-0673-y

26. Shimizu S, Takehara T, Hikita H, et al. Inhibition of autophagy potentiates the antitumor effect of the multikinase inhibitor sorafenib in hepatocellular carcinoma. *Int J Cancer*. 2012;131(3):548–557. doi:10.1002/ijc.26374

27. Zhao F, Feng G, Zhu J, et al. 3-Methyladenine-enhanced susceptibility to sorafenib in hepatocellular carcinoma cells by inhibiting autophagy. *Anticancer Drugs*. 2021;32(4):386–393. doi:10.1097/CAD.0000000000001032

28. Lee YJ, Hah YJ, Kang YN, et al. The autophagy-related marker LC3 can predict prognosis in human hepatocellular carcinoma. *PLoS One*. 2013;8(11):e81540. doi:10.1371/journal.pone.0081540

29. Xu H, Yu H, Zhang X, et al. UNC51-like kinase 1 as a potential prognostic biomarker for hepatocellular carcinoma. *Int J Clin Exp Pathol*. 2013;6(4):711–717.

30. Wu DH, Wang TT, Ruan DY, et al. Combination of ULK1 and LC3B improve prognosis assessment of hepatocellular carcinoma. *Biomed Pharmacother*. 2018;97:195–202. doi:10.1016/j.biopha.2017.10.025

31. Wang B, Kundu M. Canonical and noncanonical functions of ULK/Atg1. *Curr Opin Cell Biol*. 2017;45:47–54. doi:10.1016/j.ceb.2017.02.011

32. Nazio F, Cecconi F. Autophagy up and down by outsmarting the incredible ULK. *Autophagy*. 2017;13(5):967–968. doi:10.1080/15548627.2017.1285473

33. Zhang X, Xu Y, Ma L, et al. Essential roles of exosome and circRNA_101093 on ferroptosis desensitization in lung adenocarcinoma. *Cancer Commun*. 2022;42(4):287–313. doi:10.1002/cac2.12275

34. Yang C, Wu S, Mou Z, et al. Exosome-derived circTRPS1 promotes malignant phenotype and CD8+ T cell exhaustion in bladder cancer microenvironments. *Mol Ther*. 2022;30(3):1054–1070. doi:10.1016/j.ymthe.2022.01.022

35. Zhang F, Jiang J, Qian H, Yan Y, Xu W. Exosomal circRNA: emerging insights into cancer progression and clinical application potential. *J Hematol Oncol*. 2023;16(1):67. doi:10.1186/s13045-023-01452-2

36. Shang A, Gu C, Wang W, et al. Exosomal circPACRGL promotes progression of colorectal cancer via the miR-142-3p/miR-506-3p- TGF-beta1 axis. *mol Cancer*. 2020;19(1):117. doi:10.1186/s12943-020-01235-0

37. White E, DiPaola RS. The double-edged sword of autophagy modulation in cancer. *Clin Cancer Res*. 2009;15(17):5308–5316. doi:10.1158/1078-0432.CCR-07-5023

38. Chen Y, Li C, Tan C, Liu X. Circular RNAs: a new frontier in the study of human diseases. *J Med Genet*. 2016;53(6):359–365. doi:10.1136/jmedgenet-2016-103758

39. Memczak S, Jens M, Elefsinioti A, et al. Circular RNAs are a large class of animal RNAs with regulatory potency. *Nature*. 2013;495(7441):7441):333–8. doi:10.1038/nature11928

40. Zhang Y, Zhang XO, Chen T, et al. Circular intronic long noncoding RNAs. *Mol Cell*. 2013;51(6):792–806. doi:10.1016/j.molcel.2013.08.017

41. Li Y, Zheng Q, Bao C, et al. Circular RNA is enriched and stable in exosomes: a promising biomarker for cancer diagnosis. *Cell Res*. 2015;25(8):981–984. doi:10.1038/cr.2015.82

42. Huang D, Zhu X, Ye S, et al. Tumour circular RNAs elicit anti-tumour immunity by encoding cryptic peptides. *Nature*. 2024;625(7995):593–602.